

Microcantilever biosensor: sensing platform, surface characterization and multiscale modeling

Chuin-Shan Chen^{*1}, Shu Kuan², Tzu-Hsuan Chang¹, Chia-Ching Chou¹,
Shu-Wei Chang¹ and Long-Sun Huang²

¹Department of Civil Engineering, National Taiwan University, Taipei 10617, Taiwan

²Institute of Applied Mechanics, National Taiwan University, Taipei 10617, Taiwan

(Received August 29, 2010, Accepted May 19, 2011)

Abstract. The microcantilever (MCL) sensor is one of the most promising platforms for next-generation label-free biosensing applications. It outperforms conventional label-free detection methods in terms of portability and parallelization. In this paper, an overview of recent advances in our understanding of the coupling between biomolecular interactions and MCL responses is given. A dual compact optical MCL sensing platform was built to enable biosensing experiments both in gas-phase environments and in solutions. The thermal bimorph effect was found to be an effective nanomanipulator for the MCL platform calibration. The study of the alkanethiol self-assembly monolayer (SAM) chain length effect revealed that 1-octanethiol (C₈H₁₇SH) induced a larger deflection than that from 1-dodecanethiol (C₁₂H₂₅SH) in solutions. Using the clinically relevant biomarker C-reactive protein (CRP), we revealed that the analytical sensitivity of the MCL reached a diagnostic level of 1–500 µg/ml within a 7% coefficient of variation. Using grazing incident x-ray diffractometer (GIXRD) analysis, we found that the gold surface was dominated by the (111) crystalline plane. Moreover, using X-ray photoelectron spectroscopy (XPS) analysis, we confirmed that the Au-S covalent bonds occurred in SAM adsorption whereas CRP molecular bindings occurred in protein analysis. First principles density functional theory (DFT) simulations were also used to examine biomolecular adsorption mechanisms. Multiscale modeling was then developed to connect the interactions at the molecular level with the MCL mechanical response. The alkanethiol SAM chain length effect in air was successfully predicted using the multiscale scheme.

Keywords: microcantilever (MCL); label-free; biomolecular interaction; biosensing; self-assembly; antigen; microfluidics; x-ray photoelectron spectroscopy (XPS); multiscale modeling.

1. Introduction

The *More Than Moore's Law* movement originated from the semiconductor industry is currently flourishing around the world where the concept of system integration rather than transistor density has been highlighted (Tummala 2006). The success of the movement will highly depend on whether we can find *super* applications to create the next-level of growth in the semiconductor industry. Among many potential applications, biosensing is considered to be at the top of the list (Schultz *et al.* 2004). From a technical point of view, biosensing applications continually benefit from rapid technological advances. With the progress in micro- and nano-electromechanical systems (MEMS/NEMS) and nanotechnologies, biosensing tools continue moving towards miniaturization, high

*Corresponding Author, Professor, E-mail: dchen@ntu.edu.tw

sensitivity, portability, and wireless networking. Economically, markets associated with biosensing applications are expected to display unprecedented growth. For example, Frost & Sullivan reported that by 2012, the worldwide market for healthcare and medical devices will be worth approximately 2.6 billion US dollars (USD) in the US, 2.3 billion USD in the EU, and an additional 43.2 billion USD in the global market. The market of telemedicine and telecare devices is also expected to increase from 467 million USD in 2007 to 8 billion USD in 2012.

The microcantilever (MCL) sensor is one of the most promising platforms for next-generation label-free biosensing applications (Heath *et al.* 2009). Future biosensing applications demand portability to enable *point-of-care* personalized diagnosis and parallelization for high-throughput drug screening. Both requirements can be potentially fulfilled by the MCL. In terms of portability, the MCL benefits considerably from silicon processing with fabrication compatible with the integrated circuits (IC) industry (Fig. 1). It can be integrated into a portable *lab-on-chip* platform to enable personalized *point-of-care* diagnosis. As for parallelization, an array with hundreds or even thousands of MCL sensors can be fabricated in a batch. In light of these benefits, the MCL sensor outperforms other conventional label-free sensor technologies including surface plasmon resonance (SPR) and the quartz crystal microbalance (QCM).

The MCL technique was derived from atomic force microscopy (AFM) in the late 1980s. As the surface-to-volume ratio increases dramatically with reduced dimensions, surface effects are greatly

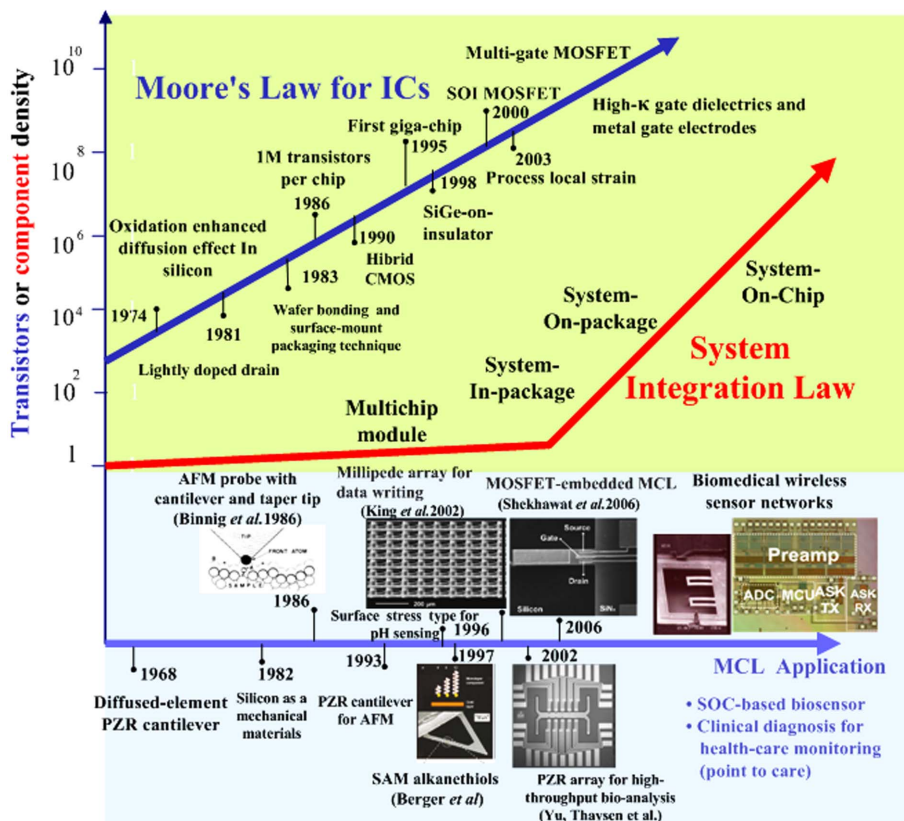


Fig. 1 Transistors and component density advances in semiconductors (above) and the advance of micro- and nano-electromechanical system (MEMS/NEMS) fabricated microcantilever (below)

amplified in the MCL. Therefore, numerous piezoresistive MCL devices have been implemented for mass sensing, chemical sensing, and also inertial sensing. For example, Barnes *et al.* (1994) measured the heat and mechanics of amalgamation by exploiting the bimetallic effect. Consequently, MCL allows the detection of relatively small surface stresses associated with the heat change to the order of picojoules (10^{-12} J) and can thus be used as a precise thermometer or calorimeter.

Given the requirement to detect single molecule in complex solutions in real-time without influencing the sample, biomolecular detection and medical diagnostic are more complex than physical or chemical sensing. A typical biosensor therefore consists of two basic components, a recognition element and a signal transducer. The recognition element is normally a receptor which can bind or interact with a target analyte (ligand) molecule. This sensing layer specifies the molecules that can interact with the sensor. The signal transducer is the read-out system. Current methods of detection and identification of biomolecular interaction include plate culture wherein the receptor is grown selectively on the substrate and identified with labeled reagents such as plaque assays and hemagglutination inhibition tests. For example, in enzyme-linked immunosorbent assay (ELISA), biospecific events are transformed into fluorescence signals. A disadvantage of labeled biosensing is the potential for possible interference occurring from the interaction. While these types of methods are well established, they are laborious and time consuming; the process routinely requires 24-48 hours (Sambrook *et al.* 2001). Moreover, as detection for disease specific biomarkers including prostate cancer, congestive heart failure, and acute myocardial infarction are moving towards ng/mL or even pg/mL, most labeled detection methods are not sensitive enough to differentiate between true signals and background readings.

The MCL is a label-free detection method which does not require intrinsic chemical selectivity. Selective chemical recognition is indirectly achieved by an affinity binding reaction where the MCL is coated with either a self-assembled monolayer (SAM; Love *et al.* 2005), a DNA probe (Hansen *et al.* 2001), an antibody (Wu *et al.* 2001a), or a peptide. Among all immobilization chemistry selections, a thin gold film is one of the best candidates for adsorption of alkanethiols in which $\text{Au}^+ - \text{S}^-$ is covalently attached in solutions or in the vapor phase. A gold film also provides a hydrophilic environment for the biomolecular interaction. Meanwhile, SAMs act as the capturing molecules, spontaneously forming uniformly ordered, densely packed and strong covalent binding monolayers, such as alkane chain molecules with thiol groups (-SH) on gold substrates, or silanes (-SiOX) on silicon substrates (Dubois *et al.* 1992). The target analyte is then modified to attach with ligands that only react with the active site. Several covalent coupling chemistries are available to immobilize the ligands. The amine (-NH₂), thiol (-SH), aldehyde (-COOH), and streptavidin-biotin coupling chemistries are well-established procedures. Covalent coupling is stable and leads to little modification of the ligands. The immobilization level can also be easily controlled and the ligand consumption is low. The immobilized sensing elements such as thiol SAMs should be robust and not easy to be removed in biosensing applications.

The controlling immobilization means that the biomolecules can be immobilized on the sensor chip surface. Due to the unbalanced surface stress caused from selective binding on one side, MCL biosensors can translate the bio-recognition events into mechanical motion ranging from a few to hundreds of nm. The MCL biosensor is a very promising technology for studying biospecific interactions in real time without labeling any of interactants. The information obtained from the MCL includes specificity, concentration, and affinity.

In this paper, an overview of recent advances in our understanding of the coupling between biomolecular interactions and MCL responses is given. We start with the MCL read-out techniques

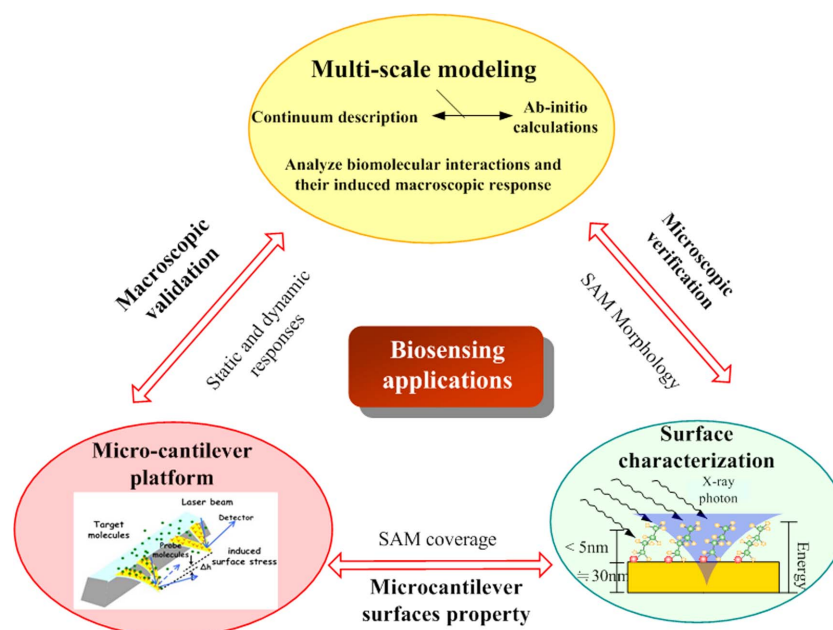


Fig. 2 The conceptual link between the MCL biosensing platform, multiscale modeling, and surface characterization

and compare their performance achieved through different biomolecular interactions. We then describe our recent activities and results in the MCL biosensing platform design and implementation, surface characterization and multiscale modeling. Multiscale modeling is developed to connect microscopic molecular interactions with macroscopic MCL mechanical responses. The MCL sensing platform and measurements provide macroscopic validation whereas the surface characterization provides microscopic verification. Putting all this together, these activities complement each other to give a full perspective on the molecular aspects of biospecific interactions and their coupling with the macroscopic MCL response (Fig. 2).

2. Overview of MCL performance

2.1 Cantilever read-out techniques

The basic MCL biosensing principle is illustrated in Fig. 3. The immobilized sensing element serves as the capturing molecule which can bind the target but does not interact with the background molecules. The block protects the sensor against nonspecific biomolecules. The MCL is a nanomechanics-based transducer with a read-out system to transform biospecific events into deflection or an electric signal. Common read-out techniques for the MCL can be classified into two broad categories: optical and electronic read-out systems.

2.1.1 Optical deflection detection

The most common method for measuring the deflection of a MCL is the optical lever technique implemented in the commercial AFM. This technique works by firing a focused laser beam to the

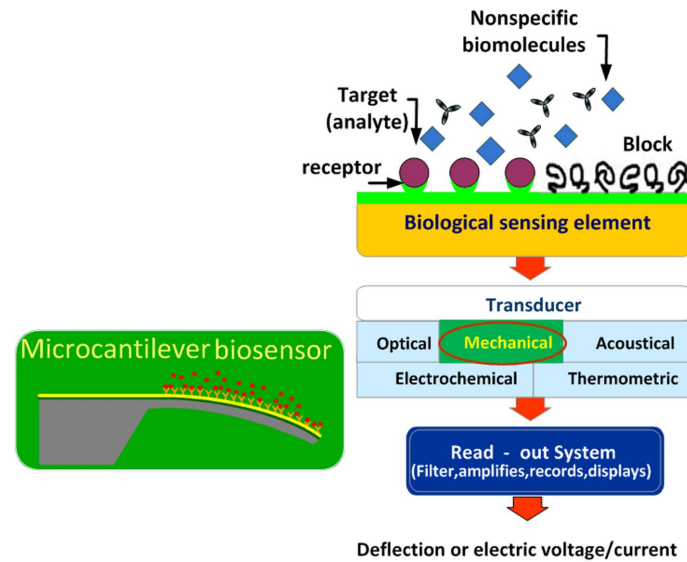


Fig. 3 Schematic representation of Biosensing principles. The immobilized sensing element serves as the capturing molecule which can bind the target but does not interact with the background molecules. The block can protect the sensor against nonspecific biomolecules

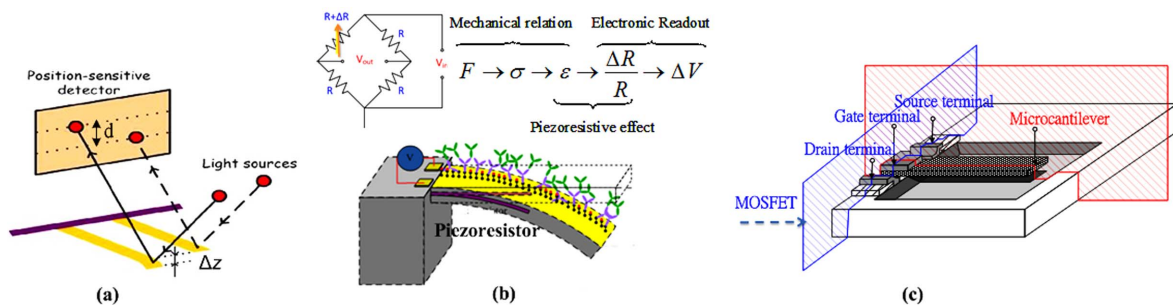


Fig. 4 Schematic illustration of the read-out system, (a) the optical read-out method, (b) the piezoresistive read-out system with a Wheatstone bridge configuration and (c) the MOSFET-embedded microcantilever

free end of the MCL. The beam reflects into a position-sensitive detector (PSD) which detects the position of the reflected laser spot, as shown in Fig. 4(a). When the MCL bends, the reflected spot moves accordingly. This movement is proportional to the MCL deflection and can be readily calculated from the motion of the spot in the PSD. Recently, Yue and colleagues (2004) have developed an array for the parallel deflection detection of hundreds of MCL sensors with a resolution range between 1-10 nm. The optical readout is based on a two-dimensional charge-coupled device (CCD). The CCD camera serves as a PSD to monitor the laser beam reflected from the MCL.

The other optical detection method is based on the interference between a reference laser beam and a sensing laser beam reflected by the tip of the MCL (Cooper *et al.* 2000). These two beams interfere and the signal can be measured using a photodiode. It is claimed to be a highly sensitive method that provides a direct and absolute deflection measurement in the 2Å range (Fernando and Austin 2009).

2.1.2 Electronic read-out deflection detection

The piezoresistive (PZR) method (Barlian *et al.* 2009) uses the embedding of a PZR material near the top surface of the MCL to measure the stress change occurring at the surface of the MCL (Fig. 4(b)). As the MCL deflects, it undergoes a stress change that will induce a strain to the piezoresistor, thereby causing a change in the resistance. The change in resistance can be read by a Wheatstone bridge circuit which converts the resistivity signal into the voltage read-out. Compactness is the major benefit gained from an electronic read-out system. As the PZR material is directly embedded in the MCL, there is no need for an extra instrument for deflection detection. Nevertheless, the fabrication of a MCL with PZR materials is relatively involved for biosensing applications. The PZR materials need to be encapsulated in a dielectric insulation layer typically made of silicon nitride or oxide ranging from tens to hundreds of nm to avoid the leakage current in solutions.

The sensitivity of the piezoresistor depends on the ratio of the gauge factor of the piezoresistor G_f and the Young's modulus E of the MCL

$$\frac{\Delta R}{R_0} = \frac{2d_n G_f \Delta z}{L^2} \propto \frac{G_f}{E} \quad (1)$$

in which ΔR is the change in resistance, R_0 is the reference resistance, d_n is the distance from the piezoresistor to the neutral axis of the MCL, Δz is the change in deflection, and L is the length of the MCL. The gauge factor G_f is defined by measuring the relative change in resistance while straining the MCL. The gauge factor varies between metals (2~5), polysilicon (20~28), and single crystalline silicon (100~200). Polysilicon is the most common piezoresistor material due to the fabrication consideration which requires no use of costly silicon on insulators. In addition, the piezoresistor materials must be carefully placed away from the neutral axis of the MCL to reach maximum sensitivity.

The well-known metal-oxide semiconductor field effect transistor (MOSFET) can also be used as an alternative electronic read-out (Fig. 4(c)). Shekhawat *et al.* (2006) and Tark *et al.* (2009) have shown that concentrations of biotin as low as 100 pg/mL can be detected using the MOSFET embedded at the base of the MCL. Since the conductivity of the MOSFET channel region is strain dependent, deflection-induced strain of the MCL due to biomolecular binding can be detected by the change in the drain current. The conversion factor for the deflection profile with respect to the change in the current can be calibrated by bending the MCL using a nanomanipulator.

2.2 MCL biosensing application and performance

MCL biosensors enable observations of biomolecular events to be made in real time. Table 1 compares the performance using different biomolecular interaction couplings with different read-out techniques over the past few years (Alvarez *et al.* 2003, Braun *et al.* 2009, Dauksaite *et al.* 2007, Desikan *et al.* 2007, Dhayal *et al.* 2006, Fritz *et al.* 2000a, Moulin *et al.* 2000, Mukhopadhyaya *et al.* 2005a,b, Ndieyira *et al.* 2008, Pei *et al.* 2004, Raiteri *et al.* 2000, Raorane *et al.* 2008a,b, Shekhawat *et al.* 2006, Thundat *et al.* 1997, Wee *et al.* 2005, Weeks *et al.* 2003, Wu *et al.* 2001b, Yang *et al.* 2003, Zhang *et al.* 2006, Zuo *et al.* 2007).

2.2.1 Genetic analysis

Nucleic acids are easy to immobilize on a gold surface when modified with a thiol group at their

Table 1 Performance using different biomolecular interactions coupled with different read-out techniques

Interaction system	Read-out Technique	Target Analyte	Lowest concentration	Reference
Thiol SAM				
	PZR	1-octanethiol, 2-octanethiol, 3-octanethiol,	1 μ M	(Desikan <i>et al.</i> 2007)
Biochemical compound				
	CCD	Toluene, DNT	50 ppb	(Raorane <i>et al.</i> 2008a)
	Optical	DDT	10 nM	(Alvarez <i>et al.</i> 2003)
	PZR	TNT	10 ppb	(Zuo <i>et al.</i> 2007)
DNA hybridization				
	Optical	mRNA	Picomolar level	(Zhang <i>et al.</i> 2006)
	PZR	DNA	0.2 μ M	(Mukhopadhyia <i>et al.</i> 2005a)
Proteins				
	PZR	human oestrogen receptor (ER α -LBD)	2.5~20 nM	(Mukhopadhyia <i>et al.</i> 2005b)
	PZR	GST protein	40 nM(1 ng/ml)	(Dauksaite <i>et al.</i> 2007)
	PZR	PSA	10 ng/ml	(Wee <i>et al.</i> 2005)
		CRP	100 ng/ml	
	CCD	Trypsin	5 nM	(Raorane <i>et al.</i> 2008b)
	MOSFET	streptavidin-biotin	100 fg/ml	(Shekhawat <i>et al.</i> 2006)
		IgG	0.1 mg/ml	
Pathogens				
	Optical	salmonella enteric(bacterial)	10 ⁶ cfu/ml	(Weeks <i>et al.</i> 2003)
	Optical and resonant mode	bacillus subtilis spores	50 spores	(Dhayal <i>et al.</i> 2006)
	CCD and resonant mode	T5 phages virus	3 pM	(Braun <i>et al.</i> 2009)
	Optical read out	vancomycin	10 nM	(Ndieyira <i>et al.</i> 2008)

5'-end. Adsorption kinetics and nanomechanical properties of thiol-modified ssDNA oligonucleotides on a gold layer were investigated with the MCL transducer by Wu *et al.* (2001b). Detection of specific hybridization of oligonucleotides to single-stranded complementary oligonucleotides functionalized on the MCL surfaces was reported by Fritz *et al.* (2000a). They also showed that the MCL biosensor can detect a single-base mismatch within 12-mer oligonucleotides. Therefore, it is possible to measure single base-pair variations in DNA (single nucleotide polymorphisms, SNP) with the MCL sensor; such a variation is the major source of several diseases.

2.2.2 Protein analysis

Protein is the fundamental bio-functional unit. The biological function of a protein is presented by its specific recognition with the ligand. Understanding the mechanisms of protein-ligand interactions is important for many applications, including biosensing, disease diagnosis, and drug discovery. The well-known biomolecular recognition of extremely high affinity, the avidin-biotin system, was investigated by Wu *et al.* (2001b). On a heparin-covered MCL, Moulin *et al.* (2000) differentiated the adsorption of low density lipoproteins from their oxidized form which are responsible for

cholesterol accumulation in arteries. Thundat *et al.* (1997) reported the deflection variation of an antibody-covered MCL as a function of time due to interactions with their specific antigens. Using this immunoassay technology in a controlled environment, Raiteri *et al.* (2000) detected the binding of a 2,4-dichlorophenoxyacetic acid (2,4-D), a commercial herbicide, from its monoclonal antibody immobilized on the MCL sensing surface.

2.2.3 Other applications

A MCL coated with a bilayer of Cu^{2+} and *L*-cysteine was reported by Yang *et al.* (2003). It is able to detect nerve agents (namely, organophosphorous compounds) due to the formation of a strong bond between the phosphonyl group and the Cu ion. Zhang *et al.* (2006) have also successfully used MCL coated with membrane-bound ligands to carry out drug screening which may provide new opportunities for drug identification in therapeutic areas. Pei *et al.* (2004) quantitatively detected the glucose level related to diabetes. Blood glucose levels are usually detected with amperometric devices, in which glucose oxidase is coupled to the electrochemical system. However, there are several interfering agents, such as ascorbic acid and many others, which are also electroactive with the applied potential. They reported that a MCL coupled to glucose oxidase underwent static bending due to a change in the surface stress when glucose was present. In contrast with amperometric devices, there was no response in the MCL to the interfering species.

3. MCL biosensing platform

In this section, we describe our recent activities in designing and implementing a robust MCL platform for biosensing applications. A compact optical MCL sensing platform integrated with a microfluidic channel was built to enable the study of biomolecular interactions in both a gas-phase and solutions.

3.1 Platform setup

A MCL biosensor consists of a MCL chip, a signal read-out module, and a flow handling system for gas or liquid environments. We designed our MCL chip to be a *V*-shaped cantilever to avoid twisting. The substrate of the MCL was a 500 nm thick low-stress silicon nitride (Si_xN_y) film which was deposited using the chemical vapor deposition process and patterned to define the MCL layout by reactive ion etching. The design and fabrication processes for the MCL are indicated in Fig. 5. Each MCL was designed to typical dimensions and was sequentially washed in a Piranha solution for 5 minutes and then rinsed with a large amount of deionized water for 10 minutes. Then, it was evaporated with a 5 nm thin chrome film as an adhesion layer followed by a 30 nm gold layer at 3×10^{-6} Torr and a rate of 0.1 nm/s on one side of the MCL.

The coating process of the gold layer is essential for reliable nanomechanical measurements. Mertens *et al.* (2007) reported that a gold film of small thicknesses and low deposition rate would exhibit the highest sensitivity and reproducibility for molecular adsorption. The process was adapted herein. The grain size and orientation of the gold surface are discussed in the following *Surface Characterization* section.

Prior to surface functionalization of the MCL with the SAM, the gold surfaces need to be carefully cleaned. In our case, they were cleaned using a UV-Ozone treatment for 10 minutes and

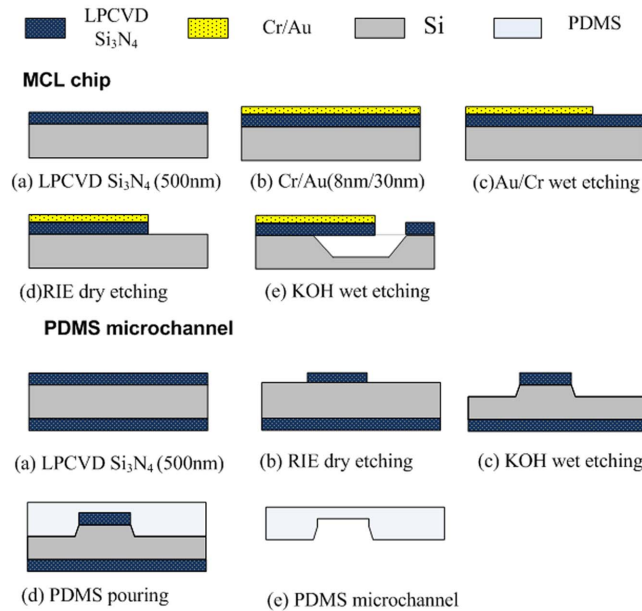


Fig. 5 The fabrication process of MCL chip and PDMS microfluidic channel

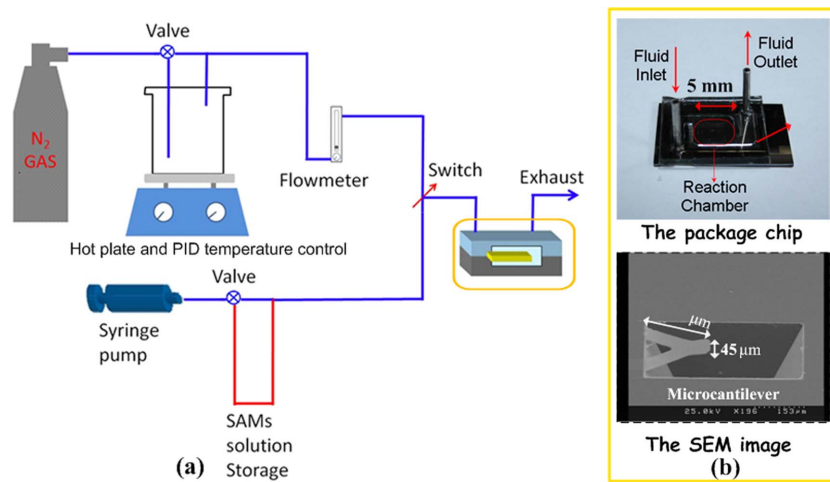


Fig. 6 (a) Illustration of the dual MCL sensing platform for conducting biosensing experiments in a gas-phase or liquid environments

soaked in pure ethanol for 20 minutes. The organic contaminants on the gold surface were oxidized to volatile products such as carbon dioxide and water. The gold oxide was reduced by ethanol oxidation (Ron *et al.* 1998). Finally, the MCL chip was mounted in a sealed microfluidic channel made of polydimethylsiloxane (PDMS) with a volume of approximately $50 \mu\text{L}$ using the surface-activated oxygen plasma process. The PDMS polymer was chosen due to its optical transparency, biocompatibility, and ease of manufacturability. After the assembly of a PDMS-based *cap* and inlet/outlet tube, the microfluidic channel for the reaction region was formed (Fig. 6(b)).

The read-out module was based on the optical lever technique. Our system included a He-Ne laser (~ 3 mW, wavelength = 633 nm) and a PSD. The fluid handling system was designed for the relatively easy study of biomolecular interactions in both liquid and gas-phase environments as shown in Fig. 6(a). To conduct sensing experiments in the liquid environment, the fluid handling system was attached to a well-controlled flow rate syringe pump (KDS 100 Syringe Pump). To carry out experiments in gas-phase environments, the fluid handling system was attached to the gas system with a buffer N_2 gas generator. During the experiment, buffers were required to continuously flow into the MCL chip until the measured signal reached a stable state.

3.2 Calibration

The correlation factor needs to be established to link between the value (d) recorded by PSD and the actual deflection (Δz) of the MCL (Fig. 4(a)). In this study, MCLs were calibrated by making use of the bimorph effect between gold and silicon nitride layers due to mismatch of well-established thermal expansion coefficients. Therefore, an imposed temperature change can bend the MCL. It thus serves as a nanomanipulator for calibration. The MCL deflection from the temperature change can be calculated from the following (Timoshenko 1925)

$$\Delta z = \frac{\frac{3L^2(\alpha_1 - \alpha_2)\Delta T}{(t_1 + t_2)} \left(1 + \frac{t_1}{t_2}\right)^2}{3\left(1 + \frac{t_1}{t_2}\right)^2 + \left(1 + \frac{t_1 E_1}{t_2 E_2}\right) \left(\frac{t_1^2}{t_2^2} + \frac{t_2 E_2}{t_1 E_1}\right)} \quad (2)$$

in which Δz is the deflection change, ΔT is the change in the imposed temperature, α is the thermal expansion coefficient, t_1 and t_2 are the thicknesses, and E_1 and E_2 are the Young's moduli of the silicon nitride and the thin gold film, respectively. The thermo-mechanical sensitivity of 160 nm/K was

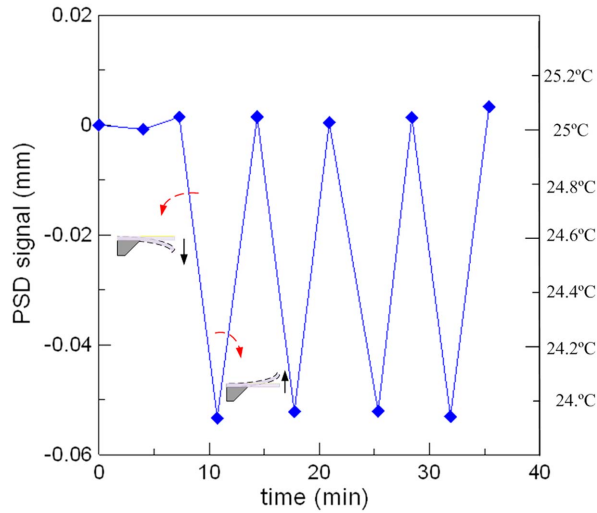


Fig. 7 The reversible and reproducible PSD responses subject to eight temperature cycles from within ± 1 °C. The initial phase to reach an equilibrium state is also shown

determined using Eq. (2). The MCL was tested in air with a thermoelectric (TE) cooler system to modulate the temperature variation. The output responses of d and temperature have been recorded within four temperature cycles between 24 to 25°C at a constant heating and cooling rate. The results were repeatable and proportional to the temperature variation, as shown in Fig. 7. Based on the 160 nm/K thermo-mechanical sensitivity, we found that 1 mm PSD value corresponded to 31376 ± 2 nm MCL deflection.

3.3 Cantilever surface functionalization

When alkanethiols are anchored to a substrate, they form so-called monolayers whereby the chains are stretched with respect to their preferred configuration and end with an appropriate functional group which can conjugate with antibody. The concept of antibody-antigen reaction is the selectivity and fitness of key (i.e., antigen) and lock (i.e., antibody). In the following, we report experiments on the adsorption of alkanethiols and macromolecules such as C-reactive protein (CRP). The former functionalizes the gold-coated MCL and the latter demonstrates potential biosensing applications using MCL.

3.3.1 Alkanethiol SAM chain length effect

The alkanethiols chain length effect on the MCL bending response in solutions under the saturation concentrations of 20 mM was studied to serve as the basis for a direct comparison with the multiscale prediction discussed later. The alkanethiols chosen herein were 1-octanethiol ($C_8H_{17}SH$) and 1-dodecanethiol ($C_{12}H_{25}SH$) (Sigma-Aldrich, Inc.). These molecules were prepared in pure ethanol (>99.8%, Sigma-Aldrich, Inc.). The microfluidic channel and reaction region were steadily immersed with a flow of pure ethanol for 30 minutes to establish a baseline. Analytic solutions were then injected into the MCL surface via a four-way valve that allowed for switching of different solutions. All experiments were performed in the liquid phase and pure ethanol was used as the carrier flow. A constant flow rate of 10 $\mu\text{L}/\text{min}$ was maintained to reduce signal fluctuation. Moreover, a TE

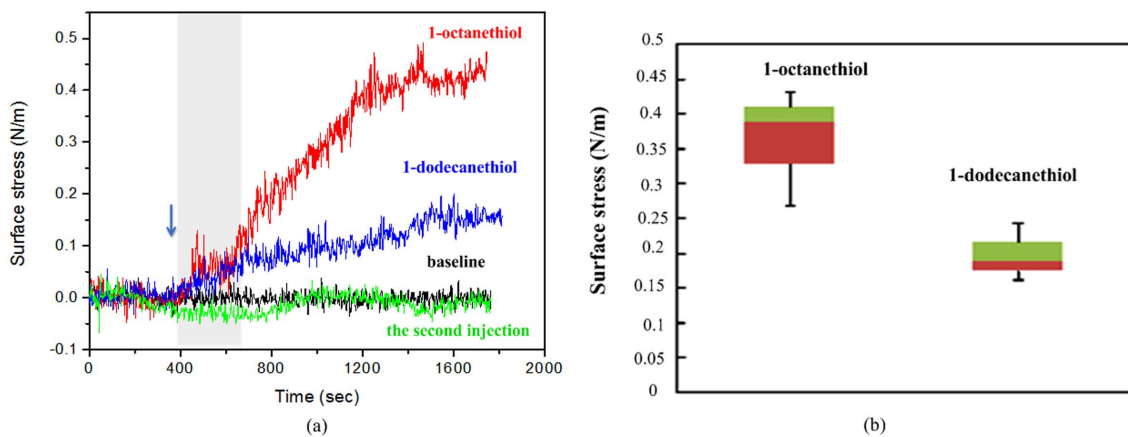


Fig. 8 (a) Surface stress variation of the MCL as a function of time to the exposure of the MCL to different chain lengths of the alkanethiol molecules. The arrow indicates the time of injection and the patterned rectangle indicates the time period when the MCL was in contact with the injected buffer and (b) The deflection of 1-octanethiol and 1-dodecanethiol in solutions

cooler and a feedback loop were used to control the temperature of the MCL device within ± 0.1 °C.

The baseline shown in Fig. 8(a) reveals the thermal and flow stability of the system. The noise in the sensing signal was approximately 0.043 N/m. The other two curves in Fig. 8(a) show the sensing response of the MCL modified with different chain lengths of the SAMs. Once the target molecules entered the reaction region, the MCL deflected upwards until the surface stress reached saturation. We injected alkanethiols twice in order to ensure that the MCL surface was filled with alkanethiols. Nearly no reaction was observed for the second injection. The surface stress of the MCL shown in Fig. 8(b) reveals that 1-octanethiol ($C_8H_{17}SH$) induces a larger deflection than 1-dodecanethiol ($C_{12}H_{25}SH$) in solutions.

3.3.2 Label-free detection of cardiac disease biomarkers C-reactive protein (CRP)

In biosensing experiments, the protein pair used herein was the human CRP (human ascites, purity $\geq 95\%$, Calbiochem Inc.) and its monoclonal anti-human CRP (mouse IgG1 isotype, Sigma Chemical Corp.). The aim of this procedure was to detect the CRP antigen molecules of the analyte (referred to as CRP below for brevity) with the MCL functionalized with the monoclonal antibody of anti-human CRP (referred to as anti-CRP below for brevity). For the anti-CRP to be successfully immobilized on the MCL surface, a series of surface modifications were required. Initially, distilled phosphate-buffered saline (PBS) solutions were injected at a constant flow rate of 10 $\mu\text{L}/\text{min}$ into the microchannel until a stable signal of the MCL was obtained. The MCL was immersed in the 20 mM SAM of a carboxylic acid-terminated alkylthiol ($\text{SH}-(\text{CH}_2)_7\text{-COOH}$) solution overnight at room temperature. An activator of an EDC/NHS mixture (N-Ethyl-N'-(3-dimethylaminopropyl)-carbodiimide hydrochloride of 75 mg/mL and N-Hydroxysuccinimide of 11.5 mg/mL) was then injected to form a covalently bondable surface for adsorption of incoming anti-CRP molecules by Amine coupling modification of the carboxymethyl groups (Johnsson *et al.* 1991). Care must be taken because the activated area of the sensor surface with no immobilized anti-CRP molecules was also capable of covalent binding to incoming CRP antigen molecules. Therefore, prior to the detection of CRP, an inactivated agent of an ethanolamine-HCl (1 M) was injected to block the functional surface of the

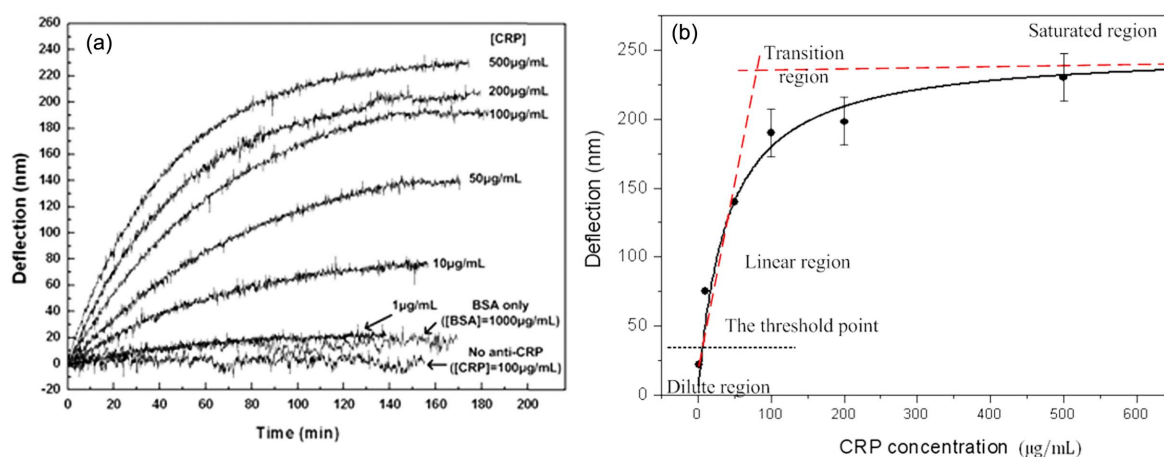


Fig. 9 (a) MCL-based CRP experiment at clinically relevant diagnostic levels: the measured deflection as a function of time at various CRP concentrations and (b) The changes in CRP induced deflection at saturation state as a function of CRP concentrations. It has achieved the lowest detected concentration of 1 $\mu\text{g}/\text{mL}$ and a diagnostic level of 1~500 $\mu\text{g}/\text{mL}$ within a 7% coefficient of variation ($n=3$)

nonspecific binding. After these procedures, the MCL biosensor was ready for specific recognition of the CRP antigen.

CRP is usually found in human serum at a concentration of less than 1 $\mu\text{g/mL}$. However, the CRP levels can rise up 100 or even 500 times during acute infection or inflammation (14 to 26 hours) anywhere in the body. It is thus a very valuable clinical risk factor for assessing cardiovascular disease (Pasceri *et al.* 2000, Ridker *et al.* 2002). Using our MCL, a wide range of clinically relevant CRP concentrations from 1 to 500 $\mu\text{g/mL}$ have been successfully measured. The results are plotted in Fig. 9. In addition, to confirm specific antigen-antibody interactions, both the unfunctionalized MCL exposed to 100 $\mu\text{g/mL}$ of the CRP antigen and the MCL functionalized with anti-CRP exposed to 1 mg/mL of bovine serum albumin without any CRP antigen were conducted. As shown in Fig. 9(a), no false positives were confirmed by the relatively insignificant MCL deflection. Fig. 9(b) shows the steady state values of surface stresses for different CRP concentrations. The solid line represents the fitting of experimental data to Langmuir adsorption isotherm. The linear range of concentration curve is between 1~50 $\mu\text{g/mL}$. The assay curve achieves the saturation level when the concentration is beyond 500 $\mu\text{g/mL}$. As a result, the sample of analyte concentrations should be adjusted to stay below the saturation limit of the assay. On the other hand, the diluted region below 1 $\mu\text{g/mL}$ deviates from the linear region and a finite threshold point for producing apparent bending is identified.

The CRP after binding can be physically dissociated from the surface of MCL by applying a low-frequency ac voltage signal (0.2 Hz, 1 V) on the surrounding nickel electrode. Our proposed method can maintain antiCRP's activity for multiple times of detection due to the absence of low-pH acids (Chen *et al.* 2009a).

4. Surface characterization

Surface characterization provides important microscopic evidence and verification on the specificity, concentration, and affinity of biomolecular interactions. Despite its importance, accurate large sampling surface characterization remains difficult to achieve. In the following section, we describe our recent efforts and results on the surface characterization of the gold film as well as composition and element characterization of the functionalized surface.

4.1 SEM and GIXRD characterization of gold film

Several factors affect the quality of the SAM formation (Love *et al.* 2005, Godin *et al.* 2004, Lee *et al.* 2003, Nagoya *et al.* 2007). Among them are the crystallinity, cleanliness, roughness, defects and grain size of the gold substrate, the nature of the adsorbate (the chain length, the functional group, etc.), the solvent (ethanol, water, etc.), the target mass transportation parameters (the immersion time, the concentration of adsorbate, etc). We report our investigation of the crystallinity and grain size of gold below.

Prior to surface functionalization, the morphology and cross section of the freshly evaporated gold thin film were examined with a scanning electron microscope (Hitachi S-4000). The grain size of the Au surface was in the range of ~20-60 nm. Furthermore, a grazing incident x-ray diffractometer (GIXRD, Japan MAC Science, MXP18) was used to analyze the crystalline structure of the Au surface. The results showed four main diffraction peaks at 2θ equal to 38.2° , 44.4° , 64.6° , and 77.5° , which correspond to the (111), (200), (220), and (311) crystalline planes of Au, respectively.

The dominant peak occurred at the (111) crystalline plane. Evidently, the perfect gold surface (111) is far from reality. The crystallinity of the Au with the highest symmetry and large grain size can be achieved by post-annealing effects and deposited conditions and will be investigated in the future.

4.2 X-ray photoelectron spectroscopy (XPS) analysis

The presence and composition of alkanethiols monolayers or the target analyte protein can be determined *in situ* using an X-ray photoelectron spectroscopy (XPS). XPS is a powerful spectroscopic technique that provides information about both the elemental composition and, more interestingly, the electronic structure of the elements. XPS analysis was performed with the Phi 5600LS instrument (Physical Electronics, Inc.) with aluminum Al K α X-ray source and a line energy of 1486 eV. The pressure in the chamber was 2×10^{-9} Torr. For XPS data analysis, we focused on studying the S2p (sensitive to alkanethiol) or N1s (sensitive to CRP and anti-CRP) peaks to probe the existence of sulfur and nitrogen. Fig. 10 plots the XPS spectra for 1-octanethiol adsorbed on the gold-coated MCL surface. A wide scan taken over the full range of 700 to 0 eV with a step size of 1 eV and pass energy of 280 eV is shown in Fig. 10(a). This range covers the signals of Au, Si, S, N, C, and O elements. The surface composition for C, O, S, and Au, expressed in terms of atomic percentage,

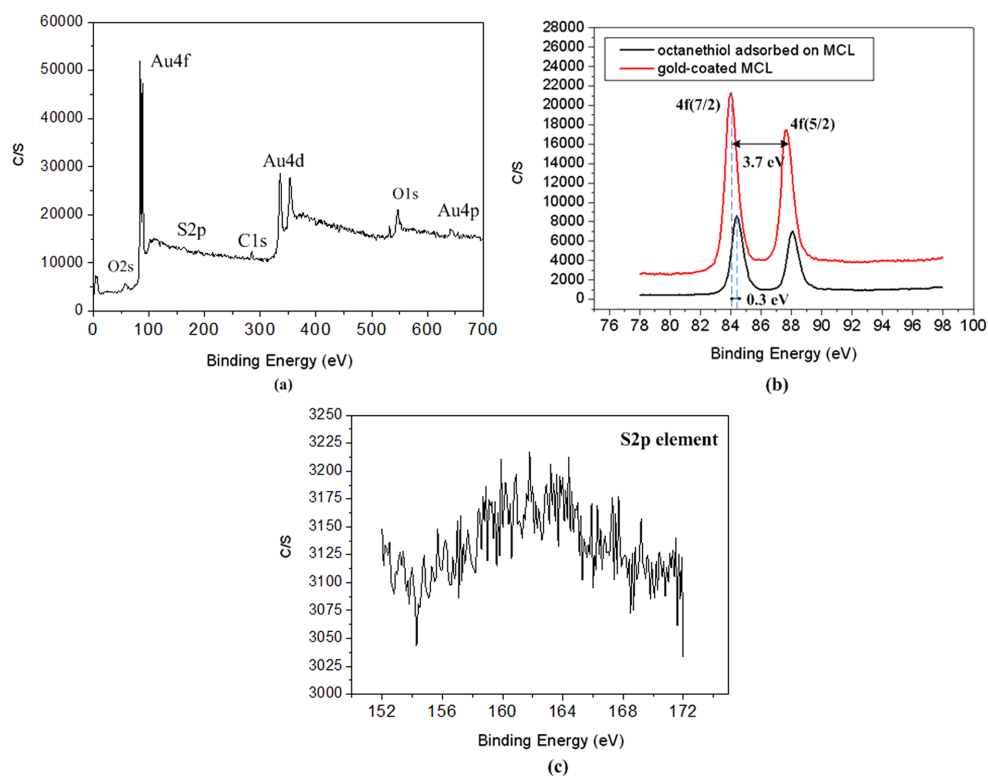


Fig. 10 XPS spectra for 1-octanethiol adsorption on a gold-coated MCL surface: (a) a wide scan with an atomic percentage of C_{1s} (30.47%), O_{1s} (13.51%), S_{2p} (3.34%), Au_{4f} (52.67%), (b) Au 4f(7/2) peak at 84.3 eV and (c) S_{2p} signal at approximately 162.3 eV

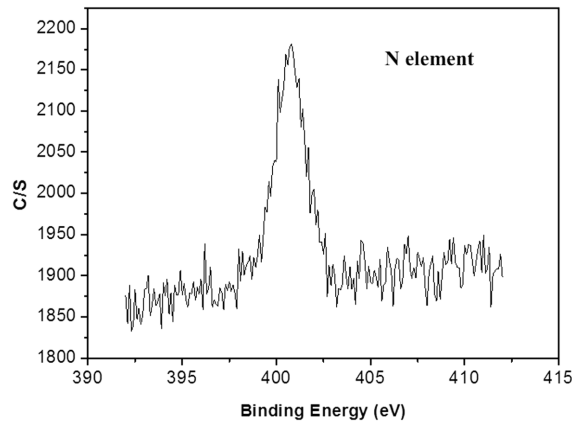


Fig. 11 The binding energy of N element at 400.6 eV after the CRP protein detection

is plotted. The binding energy (BE) scale of every spectrum was individually calibrated using the element Au 4f_{7/2} and hydrocarbon contamination emission line at 84 and 285 eV on the bare Au substrate, respectively (Moulder *et al.* 1995). It should be noted that the spin-orbit interaction causes an increase shift of 3.7 eV between Au 4f_{7/2} and 4f_{5/2}. In essence, the more bonds with electronegative atoms, the greater positive XPS chemical shifts. Figs. 10(b) and (c) plot the Au 4f_{7/2} peak at 84.3 eV (+0.3 eV shift from 84 eV) and the S2p peak at 162.3 eV (-1.7 eV shift from 164 eV). The S2p peak corresponded to the binding energy of the Au-S bond (Yang and Fan, 2002) and thus confirmed the generation of covalent bonds. Furthermore, the Au 4f_{7/2} peak intensity of modified with 1-octanethiol was significantly smaller than that of just gold-coated MCL surface where atomic percentage of Au 4f on the gold was drop from 71.23% to 52.67%. Similar to the alkanethiol spectra, we could find nitrogen N1s after the detection of the protein at a peak of about 400.6 eV (Fig. 11). Since the nonionic amine (-NH₂) occurs at 400.6~400.9 eV (Graf *et al.* 2009), this reference value supports the idea that the peak at 400.6 eV was associated with the nitrogen bond in solutions. This N1s peak provided the evidence that there were CRP molecules bonded on the MCL surface.

5. Mechanisms and multiscale modeling

The adsorption of biomolecules on a MCL surface causes the MCL to bend. The phenomenon naturally calls for multiscale modeling: we need to understand the microscopic mechanism at the molecular level and transfer critical information associated with bending deformation to the device level. The multiscale study of the MCL is fundamental to understand the mechanisms of molecular recognition and their correlation with the MCL response.

Adsorbate-induced surface stresses have been extensively studied over the past few decades (Ibach 2006). It is known that adsorption of small molecules onto a clean crystalline surface changes atomic configurations, bond angles, and electron distribution on the surface. The surface reconstruction leads to the change of the surface stress (Ibach 1997, Ibach 2006). For complex biomolecular interactions such as adsorption of protein on the MCL, mechanisms such as electrostatic, steric, and van der Waals interactions between neighboring adsorbates and conformational changes of adsorbed biomolecules have been proposed (Fritz *et al.* 2000b, Wu *et al.* 2001b, Marie *et al.* 2002). For a

solid-liquid interface covered with biomolecules, additional mechanisms such as the alternation of the electrical double layer in a buffer solution and the change of a hydrophobic to hydrophilic surface due to adsorption have been suggested (Butt 1996, Moulin *et al.* 1999, Raiteri *et al.* 2000, Fritz *et al.* 2000b, Ji *et al.* 2001). Given the diversity and complexity of biosensing applications, the aforementioned mechanisms are likely to be coupled. It remains very challenging to identify dominant mechanisms for a given biosensing application.

We have derived a multiscale modeling scheme that can analyze deformation of MCL subjected to bio-adsorption mechanisms calculated by ab-initio simulation and classical molecular dynamics (Chen *et al.* 2009b). The multiscale scheme was derived based on the minimization of the total energy with respect to the MCL curvature. The total energy contains the bending elastic energy and the energy of biomolecular adsorption as Eq. (3). The former can be obtained on the basis of the linear elastic theory (Timoshenko 1970). The latter can be calculated from atomistic simulations, for example, first-principles density functional theory (DFT) simulations (Sholl and Steckel 2009) or classical molecular dynamics simulations with proper empirical interatomic potentials (Allen and Tildesley 1989).

$$E_{total} = E_{bending} + E_{adsorption} \quad (3)$$

The bending elastic energy is

$$E_{elastic} = \frac{Y\kappa^2 t^3}{24(1-\nu^2)} bL \quad (4)$$

where Y , κ , ν , t , b and L are Yang's module, curvature, Poisson ratio, thickness, width and length of the MCL, respectively.

The equilibrium state can be obtained from that the derivative of the total energy with respect to the curvature equals to zero. From Eqs. (3) and (4), the resulting equation is

$$\sum_i^{\# atoms} \mathbf{f}_i \frac{\partial \mathbf{r}_i}{\partial \kappa} = \frac{Y\kappa t^3}{12(1-\nu^2)} b\Delta L \quad (5)$$

where the summation is the sum of the total number of atoms of a beam, and \mathbf{f}_i and \mathbf{r}_i are atomic force and position of the atom i . Thus the equation connects the microscale information (atomic force and atomic position) and macroscale physical quantity (curvature).

Using the multiscale modeling scheme, SAMs adsorbed on the MCL were modeled. The adsorption energy of SAMs on the Au(111) surface was calculated using first principles DFT simulations. The

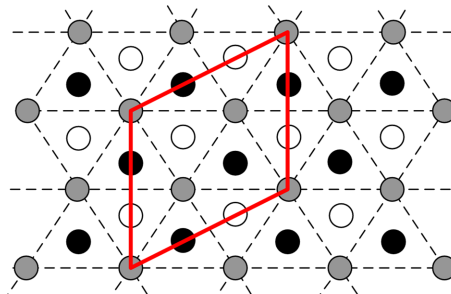


Fig. 12 The unrelaxed Au (111) surface. Three atomic layers are shown in a unit cell depicted by the red line. The gray dots indicate the atoms on the first layer, white the second layer and black the third layer

Table 2 Adsorption Results of SCH₃ on the Surface of Au(111)

	Adsorption energy (eV)	Au-S (Å)	Tilting angle	Adsorption site
Current study	-1.67	1.92	41.1	fcc
Gottschalk and Hammer 2002	-1.49	2.04	55.7	fcc
Yourdshahyan <i>et al.</i> 2002	-1.49	1.92	34.4	fcc

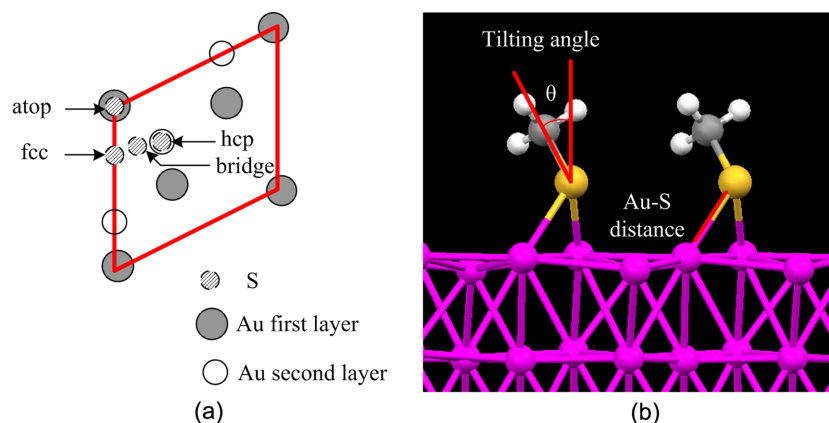


Fig. 13 (a) Adsorption sites on the x-y plane. Gray is the first layer and white is the second layer and (b) The tilting angle and Au-S distance of methanethiol (SCH₃) adsorbed on Au(111) surface

unrelaxed Au(111) surface configurations are shown in Fig. 12. The DFT total energy was calculated using the Vienna *ab-initio* Simulation Package (VASP 4.6, Kresse and Furthmüller 1996). All simulations were performed with geometry optimization using the mixture algorithm of the blocked Davidson method and the residual minimization method with direct inversion in the iterative subspace (RMM-DIIS) for the electronic relaxation, and the conjugate gradient method for the ionic relaxation.

The simulation results of methanethiol (SCH₃) adsorbed on the Au(111) surface are listed in Table 2. The results are in agreement with those from the literature (Gottschalk and Hammer 2002, Yourdshahyan and Rappe 2002). In the table, the tilting angle was measured as the S-C bond tilting an angle away from the surface normal. The Au-S was the distance between the sulfur and gold atoms in the first layer. The abridged general view is shown in Fig. 13.

The morphologies of butanethiol (SC₄H₉) and hexanethiol (SC₆H₁₃) adsorption on the gold surface were slightly different from methanethiol (SCH₃). The adsorption energies of these thiolates were 1.54 and 1.59 eV, respectively. For butanethiol (SC₄H₉) and hexanethiol (SC₆H₁₃), the adsorption site moved to the hcp site and was no longer located in the fcc site as observed from methanethiol (SCH₃). The tilting angles of butanethiol (SC₄H₉) and hexanethiol (SC₆H₁₃) were 51.9° and 64.8°, respectively. Adsorption of the thiolates affected the atomic configurations of the gold surface. The sulfur atom slightly lifted the three nearest gold atoms on the surface and induced a chain reaction to change atomic positions in the second and third layers of Au. The charge density of methanethiol (SCH₃), butanethiol (SC₄H₉) and hexanethiol (SC₆H₁₃) are shown in Fig. 14.

When the curvature was calculated from the multiscale scheme, the Au atomic forces of the first three layers dominated the results. The adsorption induces the reconstruction of the gold surface and it contributes to the curvature change. We compared the prediction with Berger's experimental data

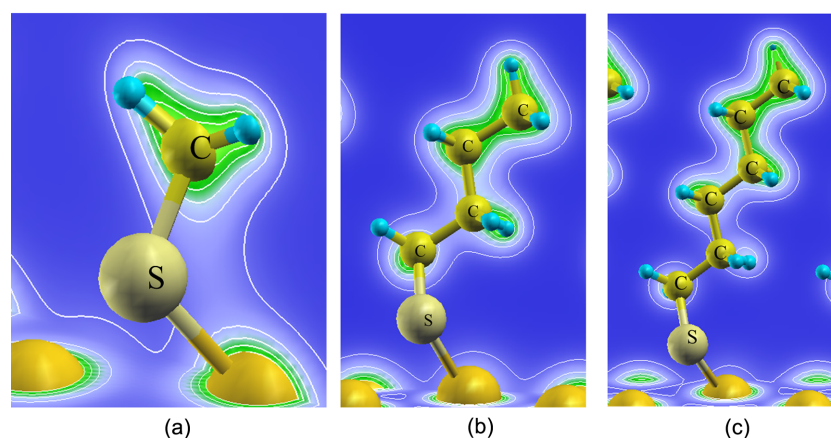


Fig. 14 Charge density distribution of (a) methanethiol (SCH_3), (b) butanethiol (SC_4H_9) and (c) hexanethiol (SC_6H_{13}) adsorbed on the Au (111) surface

(Berger *et al.* 1997). The trend of surface stress matched well as the longer the thiolate length, the larger the compressive surface stress (Chen *et al.* 2009b). Extensions of this multi-scale method to handle a more complex adsorption induced bending deformation are underway. We envision that the multiscale modeling developed herein will enable the quantitative analysis and design of the MCL in the future.

6. Conclusions

A broad overview of our recent advances in the understanding of the coupling between biomolecular interactions and MCL mechanical responses has been given. A compact optical MCL sensing platform was built to conduct biosensing experiments in both gas-phase and liquid environments. The thermal bimorph effect was found to be an effective nanomanipulator for the MCL platform calibration. Two biosensing experiments were conducted; one analyzed the effect of alkanethiol SAM chain length while the other tested the clinically relevant biomarker CRP. Full coverage of the alkanethiols on the MCL surface was confirmed by nearly no deflection responses from the second injection. We found that the 1-octanethiol ($\text{C}_8\text{H}_{17}\text{SH}$) induced a larger deflection than that from 1-dodecanethiol ($\text{C}_{12}\text{H}_{25}\text{SH}$) in solutions. In addition, CRP specificity was confirmed by exposing the unfunctionalized MCL to 100 $\mu\text{g}/\text{mL}$ of the CRP antigen and the MCL functionalized with anti-CRP to 1 mg/mL of bovine serum albumin (BSA) without CRP antigen. We found that the analytical sensitivity of the MCL achieved a diagnostic level of 1~500 $\mu\text{g}/\text{mL}$ within a 7% coefficient of variation. The CRP diagnostic level achieved by the MCL provides a very valuable clinical risk factor for assessing cardiovascular disease in the future. Using the GIXRD analysis, we found that the gold surface was dominated by the (111) crystalline plane. Using XPS analysis, we also confirmed that the Au-S covalent bonds occurred in SAM adsorption whereas CRP molecular bindings occurred in protein analysis.

A future trend in developing the next-generation of MCL biosensing is to predict, rather than to describe the MCL response. Due to the diversity and complexity of biosensing applications, it remains very challenging to identify dominant mechanisms and to furthermore correlate the mechanisms

to the MCL response. In this study, first principles DFT simulations were used to examine biomolecular adsorption mechanisms. Multiscale modeling was developed to connect the interactions at the molecular level with the MCL mechanical response. The alkanethiol SAM chain length effect in air was successfully predicted using the multiscale scheme. Critical experiments were conducted.

The electronic read-out module offers the benefit of miniaturization for the MCL platform. Future work will undoubtedly integrate the module into a system-on-chip with signal conditioning and a wireless sensor network using the complementary metal-oxide semiconductor fabrication technology. This system integration trend echoes the *More Than Moore's Law* movement and will extend the molecular diagnostics limits and enable *point-of-care* diagnosis as well as the development of personalized medicine in the future.

Acknowledgements

The research was supported by the National Science Council (NSC) of Taiwan under award no. 96-2120-M-002-002, 98-2221-E-002-108, and 98-2220-E-002-027, and 99-2627-E-002-002. We are grateful to the National Center for High-performance Computing (NCHC) for providing the computational resources.

References

- Allen, M.P. and Tildesley, D.J. (1989), *Computer Simulation of Liquids*. Oxford University Press, USA.
- Alvarez, M., Calle, A., Tamayo, J., Lechuga, L.M., Abad, A. and Montoya, A. (2003), "Development of nanomechanical biosensors for detection of the pesticide DDT", *Biosens. Bioelectron.*, **18**(5-6), 649-653.
- Barlian, A.A., Park, W.T., Mallon, J.R., Rastegar, A.J. and Pruitt, B.L. (2009), "Review: semiconductor piezoresistance for microsystems", *Proceedings of the IEEE*, **97**(3), 513-552.
- Barnes, J.R., Stephenson, R.J., Welland, M.E., Gerbert, Ch. and Gimzewski, J.K. (1994), "Photothermal spectroscopy with femtojoule sensitivity using a micromechanical device", *Nature*, **372**, 79-81.
- Berger, R., Delamar, E., Lang, H.P., Gerber, C., Gimzewski, J.K., Meyer, E. and Guntherodt, H.J. (1997), "Surface stress in the self-assembly of alkanethiols on gold", *Science*, **276**, 2021-2024.
- Braun, T., Ghatkesar, M.K., Backmann, N., Grange, W., Boulanger, P., Letellier, L., Lang, H.P., Bietsch, A., Gerber, C. and Hegner, M. (2009), "Quantitative time-resolved measurement of membrane protein-ligand interactions using microcantilever array sensors", *Nat. Nanotechnol.*, **4**, 179-185.
- Butt, H.J. (1996), "A sensitive method to measure changes in the surface stress of solids", *J. Colloid Interf. Sci.*, **180**(1), 251-260.
- Chen, C.H., Hwang, R.Z., Huang, L.S., Lin, S.M., Chen, H.C., Yang, Y.C., Lin, Y.T., Yu, S.A., Lin, Y.S., Wang, Y.H., Chou, N.K. and Lu, S.S. (2009a), "A wireless bio-MEMS sensor for C-reactive protein detection based on nanomechanics", *IEEE T. Bio. Eng.*, **56**(2), 462-470.
- Chen, C.S., Chou, C.C. and Chang, S.W. (2009b), "Ab-initio and multiscale study of surface stresses from alkanethiolate self-assembled monolayers on gold", ISCM II & EPMESC XII, November 30-December 3, Hong Kong and Macao.
- Cooper, E.B., Post, E.R., Griffith, S., Levitan, J., Manalis, S.R., Schmidt, M.A. and Quate, C.F. (2000), "High-resolution micromachined interferometric accelerometer", *Appl. Phys. Lett.*, **76**, 3316-3318.
- Dauksaite, V., Lorentzen, M., Besenbacher, F. and Kjems, J. (2007), "Antibody-based protein detection using piezoresistive cantilever arrays", *Nanotechnology*, **18**(12), 125503.
- Desikan, R., Armel, S. Meyer III, H.M. Thundat, T. (2007), "Effect of chain length on nanomechanics of alkanethiol self-assembly", *Nanotechnology*, **18**(42), 424028.
- Dhaval, B., Henne, W.A., Doorneweerd, D.D., Reifengerger, R.G. and Low, P.S. (2006), "Detection of *Bacillus subtilis* spores using peptide-functionalized cantilever arrays", *J. Am. Chem. Soc.*, **128**(11), 3716-3721.

- Dubois, L.H. and Nuzzo, R.G. (1992), "Synthesis, structure, and properties of model organic-surfaces", *Annu. Rev. Phys. Chem.*, **43**, 437-463.
- Fernando, S. and Austin, M.W. (2009), "Extending the deflection measurement range of interferometric microcantilever arrays", *J. Microelectromech. S.*, **18**, 480-487.
- Fritz, J., Baller, M.K., Lang, H.P., Rothuizen, H., Vettiger, P., Meyer, E., Guntherodt, H.J., Gerber, Ch. and Gimzewski, J.K. (2000a), "Translating biomolecular recognition into nanomechanics", *Science*, **288**, 316-318.
- Fritz, J., Baller, M.K., Lang, H.P., Strunz, T., Meyer, E., Guntherodt, H.J., Delamarche, E., Gerber, Ch. and Gimzewski, J.K. (2000b), "Stress at the solid-liquid interface of self-assembled monolayers on gold investigated with a nanomechanical sensor", *Langmuir*, **16**(25), 9694-9696.
- Godin, M., Williams, P.J., Tabard-Cossa, V., Laroche, O., Beaulieu, L.Y., Lennox, R.B. and Grutter, P. (2004), "Surface stress, kinetics, and structure of alkanethiol self-assembled monolayers", *Langmuir*, **20**(17), 7090-7096.
- Gottschalk, J. and Hammer, B. (2002), "A density functional theory study of the adsorption of sulfur, mercapto, and methylthiolate on Au(111)", *J. Chem. Phys.*, **116**, 784.
- Graf, N., Yegen, E., Gross, T., Lippitz, A., Weigel, W., Krakert, S., Terfort, A. and Unger, W.E.S. (2009), "XPS and NEXAFS studies of aliphatic and aromatic amine species on functionalized surfaces", *Surf. Sci.*, **603**(18), 2849-2860.
- Hansen, K.M., Ji, H.F., Wu, G.H., Datar, R., Cote, R., Majumdar, A. and Thundat, T. (2001), "Cantilever-based optical deflection assay for discrimination of DNA single-nucleotide mismatches", *Anal. Chem.*, **73**(7), 1567-1571.
- Heath, J.R., Davis, M.E. and Hood, L. (2009), "Nanomedicine targets cancer", *Sci. Am.*, **300**(2), 44-51.
- Ibach, H. (1997), "The role of surface stress in reconstruction, epitaxial growth and stabilization of mesoscopic structures", *Surf. Sci. Rep.*, **29**(5-6), 195-263.
- Ibach, H. (2006), *Physics of Surfaces and Interfaces*. Springer.
- Ji, H.F., Hansen, K.M., Hu, Z. and Thundat, T. (2001), "Detection of pH variation using modified microcantilever sensors", *Sensor. Actuat. B-Chem.*, **72**(3), 233-238.
- Johnsson, B., Lofas, S. and Lindquist, G. (1991), "Immobilization of proteins to a carboxymethyl-dextran-modified gold surface-for biospecific interaction analysis in surface-plasmon resonance sensors", *Anal. Biochem.*, **198**(2), 268-277.
- Kresse, G. and Furthmüller, J. (1996), "Efficient iterative schemes for ab initio total-energy calculations using a plane-wave basis set", *Phys. Rev. B*, **54**(16), 11169-11186.
- Lee, S.Y., Noh, J., Ito, E., Lee, H. and Hara, M. (2003), "Solvent effect on formation of cysteamine self-assembled monolayers on Au(111)", *Jpn. J. Appl. Phys.*, **42**(1), 236-241.
- Love, J.C., Estroff, L.A., Kriebel, J.K., Nuzzo, R.G. and Whitesides, G.M. (2005), "Self-assembled monolayers of thiolates on metals as a form of nanotechnology", *Chem. Rev.*, **105**(4), 1103-1169.
- Marie, R., Jensenius, H., Thaysen, J., Christensen, C.B. and Boisen, A. (2002), "Adsorption kinetics and mechanical properties of thiol-modified DNA-oligos on gold investigated by microcantilever sensors", *Ultramicroscopy*, **91**(1-4), 29-36.
- Mertens, J., Calleja, M., Ramos, D., Taryn, A. and Tamayo, J. (2007), "Role of the gold film nanostructure on the nanomechanical response of microcantilever sensors", *J. Appl. Phys.*, **101**(3), 034904.
- Moulder, J.F., Chastain, J. and King, R.C. (1995), "Handbook of x-ray photoelectron spectroscopy : a reference book of standard spectra for identification and interpretation of XPS data", Physical Electronics, Eden Prairie, Minn.
- Moulin, A.M., O'Shea, S.J. and Welland, M.E. (2000), "Microcantilever-based biosensors", *Ultramicroscopy*, **82**(1-4), 23-31.
- Mukhopadhyay, R., Lorentzen, M., Kjems, J. and Besenbacher, F. (2005a), "Nanomechanical sensing of DNA sequences using piezoresistive cantilevers", *Langmuir*, **21**(18), 8400-8408.
- Mukhopadhyay, R., Sumbayev, V.V., Lorentzen, M., Kjems, J., Andreasen, P.A. and Besenbacher, F. (2005b), "Cantilever sensor for nanomechanical detection of specific protein conformations", *Nano Lett.*, **5**(12), 2385-2388.
- Nagoya, A. and Morikawa, Y. (2007), "Adsorption states of methylthiolate on the Au(111) surface", *J. Phys.-Condens. Mat.*, **19**(36), 365245.
- Ndieyira, J.W., Watari, M., Barrera, A.D., Zhou, D., Vogtli, M., Batchelor, M., Cooper, M.A., Strunz, T., Horton, M.A., Abell, C., Rayment, T., Aepli, G. and McKendry, R.A. (2008), "Nanomechanical detection of antibiotic mucopeptide binding in a model for superbug drug resistance", *Nat. Nanotechnol.*, **3**, 691-696.

- Pasceri, V., Willerson, J.T. and Yeh, E.T.H. (2000), "Direct proinflammatory effect of C-reactive protein on human endothelial cells", *Circulation*, **102**, 2165-2168.
- Pei, J.H. Tian, F. and Thundat, T. (2004), "Glucose biosensor based on the microcantilever", *Anal. Chem.*, **76**, 292-297.
- Raiteri, R., Butt, H.J. and Grattarola, M. (2000), "Changes in surface stress at the liquid/solid interface measured with a microcantilever", *Electrochim. Acta*, **46**(2-3), 157-163.
- Raorane, D., Lim, S.H.S. and Majumdar, A. (2008a), "Nanomechanical assay to investigate the selectivity of binding interactions between volatile benzene derivatives", *Nano Lett.*, **8**(8), 2229-2235.
- Raorane, D.A., Lim, M.D., Chen, F.F., Craik, C.S. and Majumdar, A. (2008b), "Quantitative and label-free technique for measuring protease activity and inhibition using a microfluidic cantilever array", *Nano Lett.*, **8**(9), 2968-2974.
- Ridker, P.M., Rifai, N., Rose, L., Buring, J.E. and Cook, N.R. (2002), "Comparison of C-reactive protein and low-density lipoprotein cholesterol levels in the prediction of first cardiovascular events", *New Eng. J. Med.*, **347**, 1557-1565.
- Ron, H., Matlis, S. and Rubinstein, I. (1998), "Self-assembled monolayers on oxidized metals. 2. Gold surface oxidative pretreatment, monolayer properties, and depression formation", *Langmuir*, **14**(5), 1116-1121.
- Sambrook, J., Russell, D.W. (2001), "Molecular cloning: a laboratory manual", *Cold Spring Harbor Laboratory Press*, Cold Spring Harbor, N.Y.
- Schultz, J., Mrksich, M., Bhatia, S.N., Brady, D.J., Ricco, A.J., Walt, D.R. and Wilkins, C.L. (2004), "International research and development in biosensing", WTEC Panel Report, 283 pages.
- Shekhawat, G., Tark, S.H., Dravid, V.P. (2006), "MOSFET-embedded microcantilevers for measuring deflection in biomolecular sensors", *Science*, **311**, 1592-1595.
- Sholl, D. and Steckel, J.A. (2009), *Density Functional Theory: A Practical Introduction*. Wiley-Interscience, USA.
- Tark, S.H., Srivastava, A., Chou, S., Shekhawat, G. and Dravid, V.P. (2009), "Nanomechanoelectronic signal transduction scheme with metal-oxide-semiconductor field-effect transistor-embedded microcantilevers", *Appl. Phys. Lett.*, **94**, 104101.
- Thundat, T., Oden, P.I. and Warmack, R.J. (1997), "Microcantilever sensors", *Micro. Thermophys. Eng.*, **1**(3), 185-199.
- Timoshenko, S.P. (1925), "Analysis of bi-metal thermostats", *J. Opt. Soc. Am.*, **11**, 233-255.
- Timoshenko, S.P. (1970), *Theory of Elasticity*, 3rd Ed., McGraw-Hill Companies.
- Tummala, R.R. (2006), "Moore's law meets its match", *IEEE Spectrum*, **43**(6), 44-49.
- Wee, K.W., Kang, G.Y., Park, J., Kang, J.Y., Yoon, D.S., Park, J.H. and Kim, T.S. (2005), "Novel electrical detection of label-free disease marker proteins using piezoresistive self-sensing micro-cantilevers", *Biosens. Bioelectron.*, **20**, 1932-1938.
- Weeks, B.L., Camarero, J., Noy, A., Miller, A.E., Stanker, L. and De Yoreo, J.J. (2003), "A microcantileverbased pathogen detector", *Scanning*, **25**, 297-299.
- Wu, G.H., Datar, R.H., Hansen, K.M., Thundat, T., Cote, R.J. and Majumdar, A. (2001a), "Bioassay of prostatespecific antigen (PSA) using microcantilevers", *Nature Biotechnology*, **19**, 856-860.
- Wu, G.H., Ji, H.F., Hansen, K., Thundat, T., Datar, R., Cote, R., Hagan, M.F., Chakraborty, A.K. and Majumdar, A. (2001b), "Origin of nanomechanical cantilever motion generated from biomolecular interactions", *Proceedings of the National Academy of Sciences of the United States of America*, **98**, 1560-1564.
- Yang, Y.W. and Fan, L.J. (2002), "High-resolution XPS study of decanethiol on Au(111): Single sulfur-gold bonding interaction", *Langmuir*, **18**(4), 1157-1164.
- Yang, Y.M., Ji, H.F. and Thundat, T. (2003), "Nerve agents detection using a Cu²⁺/L-cysteine bilayer-coated Microcantilever", *J. Am. Chem. Soc.*, **125**(5), 1124-1125.
- Yourdshahyan, Y. and Rappe and Andrew M. (2002), "Structure and energetics of alkanethiol adsorption on the Au(111) surface", *J. Chem. Phys.*, **117**(2), 825-833.
- Zhang, J., Lang, H.P., Huber, F., Bietsch, A., Grange, W., Certa, U., McKendry, R., Guntgerodt, H.J., Hegner, M. and Gerber, Ch. (2006), "Rapid and label-free nanomechanical detection of biomarker transcripts in human RNA", *Nature Nanotechnology*, **1**, 214-220.
- Zuo, G.M., Li, X.X., Zhang, Z.X., Yang, T.T., Wang, Y.L., Cheng, Z.X. and Feng, S.L. (2007), "Dual-SAM functionalization on integrated cantilevers for specific trace-explosive sensing and non-specific adsorption suppression", *Nanotechnology*, **18**(25), 255501.